Exact analog of the Hatano-Nelson model in one-dimensional continuous nonreciprocal systems

A Maddi, Yves Aurégan, Guillaume Penelet, V Pagneux, V. Achilleos

Letter

Exact analog of the Hatano-Nelson model in one-dimensional continuous nonreciprocal systems

A. Maddi, Y. Auregan, G. Penelet, V. Pagneux, and V. Achilleos
Laboratoire d'Acoustique de l'Université du Mans (LAUM), UMR 6613, Institut d'Acoustique - Graduate School (IA-GS), CNRS, Le Mans Université, Le Mans, France

(Received 27 August 2023; revised 24 October 2023; accepted 13 November 2023; published 15 March 2024)

Non-Hermitian topology offers a promising avenue toward an enhanced control of waves, and many of the underlying interesting phenomena are studied through the paradigmatic Hatano-Nelson (HN) model, which remains unexplored in continuous wave systems. Herein, we propose a framework to map one-dimensional continuous nonreciprocal systems onto the HN model. Our approach, based on the properties of transfer matrices, is applicable across various physical domains. We experimentally apply our method in audible acoustics using active elements, where we not only observe the predicted skin effect but also access the spectrum topology using stable configurations and observe its subsequent boundary sensitivity. By establishing a connection between continuous wave systems and the discrete HN model, our results significantly broaden the potential application of nonreciprocal topological phenomena.

DOI: 10.1103/PhysRevResearch.6.L012061

Introduction. The intriguing characteristics of non-Hermitian Hamiltonians have attracted a lot of attention lately [1,2]. These Hamiltonians make it possible to examine nonconservative systems with complex eigenvalues. Growing interest in these systems is a result of the groundbreaking work on parity-time ($\mathcal{PT}$) symmetry [3,4], which showed that non-Hermitian systems with simultaneous parity and time symmetry could display real eigenvalues and illuminated the significance of exceptional points. Later, $\mathcal{PT}$-symmetric systems were found to have a variety of unique characteristics, including special sensitivity [5–8], coherent perfect absorption (CPA)-lasing [9–13], and unidirectional invisibility [14,15].

Inevitably, given its potential for the unidirectional control of waves and the development of sensors, non-Hermiticity is now also studied in the framework of topological phenomena [16–25]. In that regard, the topological invariants typically used to connect a lattice's bulk characteristics and its behavior near the edges of a finite system had to be reinterpreted. As a result, several concepts, including the Brillouin zone, have been redefined, and the notions of point and line gaps are now necessary to categorize the various topological classes [26]. One of the most profound discoveries of non-Hermitian topology is the non-Hermitian skin effect (NHSE) [27–29], which occurs when transitioning from periodic boundary conditions (PBCs) to open boundary conditions (OBCs) leading to the localization of bulk modes at one boundary. This effect has been extensively studied theoretically with experimental demonstration in electrical circuits [30–32] and acoustic setups [33,34].

Unquestionably, one of the most prominent models in non-Hermitian topology is the Hatano-Nelson (HN) model [35]. It consists of a one-dimensional (1D) lattice with asymmetric (nonreciprocal) hoppings which are responsible for the localization of all the bulk states at the edges, leading to the emergence of the non-Hermitian skin effect. Additionally, a field of non-Hermitian topology in discrete lattices has emerged since the recent work in Ref. [36] due to the model's topological features and those of its generalizations [25,26,28]. It has been established that these systems can be constructed in passive lossy systems [34,37]. Similarly, these models can be implemented using nonreciprocal systems, requiring the introduction of an external energy source or sink, thus potentially leading to the generation of unwanted instabilities.

In this Research Letter, we propose a comprehensive, broadband, and exact mapping of the HN model to 1D *continuous* and nonreciprocal periodic systems. To experimentally validate our theoretical model, we use an acoustic network employing active loudspeakers [38], where we observe the NHSE. Additionally, owing to the inherent system's losses, our setup remains stable under PBCs, which allows us to highlight experimentally the transition from PBCs to OBCs by using various diaphragms and exhibit the exponential sensitivity of the system to changes in boundaries.

Mapping of continuous systems. We consider the propagation of waves in a 1D periodic and continuous medium, where only plane waves are propagating (monomode approximation). Such a two-port unit cell can be described using a 2×2 transfer matrix $\mathbf{M}$ which makes a relation between two successive cells and has the general form [see also Fig. 1(a)]

$$\mathbf{M} = \begin{pmatrix} a & b \\ c & d \end{pmatrix}, \quad \det(\mathbf{M}) = t. \tag{1}$$

The state vector of the system at the position x takes the form $[A(x), B(x)]^T$, and for simplicity below we use the notation $A_n \equiv A(x_n)$. Equation (1) allows us to write the following

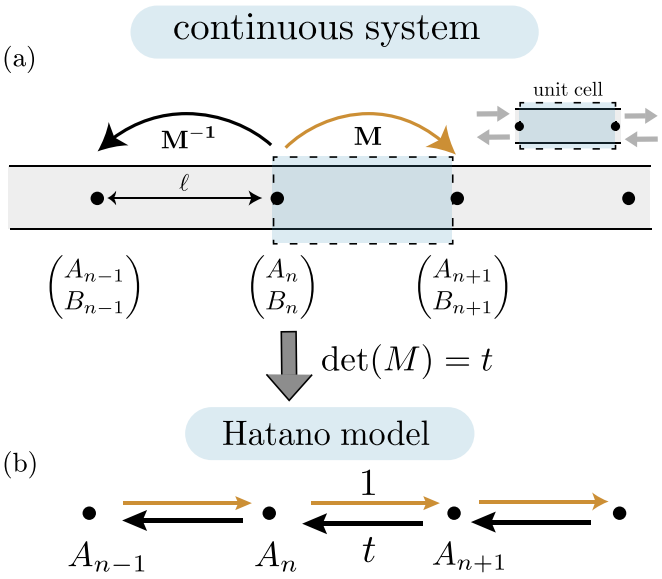

FIG. 1. (a) A sketch of a continuous system which is composed of periodically arranged unit cells of length ℓ. The edges of each unit cell are connected via the transfer matrix $\mathbf{M}$. (b) By a simple manipulation of the transfer matrix equations we map the continuous system to the HN model where the nonreciprocal coupling strength t is equal to the determinant of the transfer matrix.

system of equations between three consecutive equidistant points:

$$\begin{pmatrix} A_{n+1} \\ B_{n+1} \end{pmatrix} = \mathbf{M}\begin{pmatrix} A_n \\ B_n \end{pmatrix}, \quad \begin{pmatrix} A_{n-1} \\ B_{n-1} \end{pmatrix} = \mathbf{M}^{-1}\begin{pmatrix} A_n \\ B_n \end{pmatrix}. \tag{2}$$

The first line of each of the above systems of equations is explicitly written as

$$A_{n+1} = aA_n + bB_n, \tag{3}$$

$$tA_{n-1} = dA_n - bB_n. \tag{4}$$

Therefore, by adding the two equations (3) and (4), the problem can be simplified to the following discrete equation:

$$A_{n+1} + tA_{n-1} = EA_n. \tag{5}$$

The last equation provides an exact analog of the HN model and can be readily applied to various continuous physical systems. Note that the same equation is also true for B_n.

According to our mapping the transfer matrices of both the continuous and the discrete unit cell have the same nonunitary determinant, which was recently shown in Ref. [39] to be the key parameter to reestablish the bulk-boundary correspondence for non-Hermitian systems. The *energy* E in Eq. (5) is simply given by

$$E = \mathrm{tr}(\mathbf{M}) = a + d \tag{6}$$

and provides the direct link between the eigenvalues of Eq. (5) and the elements of $\mathbf{M}$. In practice, for wave systems the only restriction of our model is that the determinant t of the transfer matrix does not depend on the frequency. When the latter is satisfied, our exact analog of the HN is broadband and only requires periodicity and the monomode approximation.

Properties of the model. We now briefly summarize the properties of the HN model starting from the dispersion relation equation (5), which yields

$$E_q = (1+t)\cos(q) + i(1-t)\sin(q). \tag{7}$$

When $t \neq 1$, in the presence of nonreciprocity, the energies are complex. Furthermore, $E(q)$ creates a closed loop in the complex plane for $q \in [-\pi/2, \pi/2]$. The fact that the energy itself is a complex function has motivated researchers to attribute topological properties to such non-Hermitian models. In particular, it is now well established that one can define the following winding number:

$$w_E = \frac{1}{2\pi}\oint_C \frac{d}{dz}\arg E(z), \tag{8}$$

where $z = \exp(iq)$. This integral along the Brillouin zone gives $w_E = 1$ ($w_E = -1$) for $|t| > 1$ ($|t| < 1$) signaling a transition at $t = 1$. This transition is now known to be related to the appearance of the so-called skin modes [40], i.e., localized modes at one edge of a finite structure. The sign of the winding number indicates the side of localization. However, the complex spectrum of the HN (and many other non-Hermitian topological models) predicts *unstable* modes with a positive imaginary part. Such instability manifests itself in periodic systems, where initially some eigenvalues are degenerate (of order 2) for a symmetrical hopping factor $t = 1$ and lie in the complex plane. The introduction of nonreciprocity $t \neq 1$ causes the modes to split and form an ellipse characterized by unstable and damped modes. Moreover, the corresponding eigenvectors take the form

$$A_j = \frac{1}{N}[1, \lambda^j, \lambda^{2j}, \ldots, \lambda^{(N-1)j}]^T, \quad \lambda = e^{i\frac{2\pi}{N}}, \tag{9}$$

which corresponds to traveling waves. Note that these modes are different from the ones found around chiral exceptional points [41–43]. This makes it difficult to implement PBCs in a classical wave system. Our model surpasses this difficulty as long as the effects of losses are counterbalancing the instability growth.

Application to acoustics and experimental results. We now apply our theory using an acoustic system where we identify the acoustic flux $A \to u$ and pressure $B \to p$ in Eq. (1). Nonreciprocity in acoustics can be achieved using (among others) nonlinearity, active elements, spatiotemporal modulations, or the thermoacoustic effect [44–53], and here we choose a simple active element to get $|t| \neq 1$.

A sketch of the unit cell is displayed in Fig. 2(a) and consists of a cavity connected to two ducts. A speaker is installed in the center of the cavity and is controlled by a feedback loop consisting of a current amplifier and a microphone mounted in the vicinity of the loudspeaker.

The nonreciprocity arises from the electroacoustic feedback loop, in which an electrical current supplied to the loudspeaker is proportional to the feedback gain G and the pressure measured by a nearby microphone. This generates an additional oscillating force that acts on the loudspeaker membrane. For frequencies below the cutoff, the acoustic pressure and velocity at the edges of the unit cell are connected through a transfer matrix $\mathbf{M}$ as in Eq. (1), and the hopping parameter t is simply adjusted by the amplifier gain G. For a more detailed

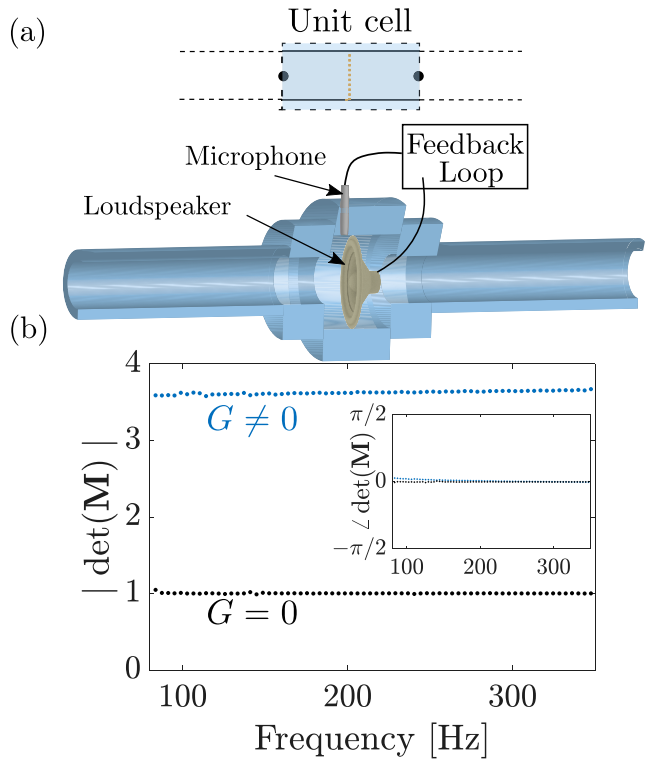

FIG. 2. (a) Sketch of the unit cell. (b) Determinant of the transfer matrix of the unit cell (equivalently, the hopping factor t) as a function of the frequency, where solid black and blue circles represent the passive and the active cell, respectively.

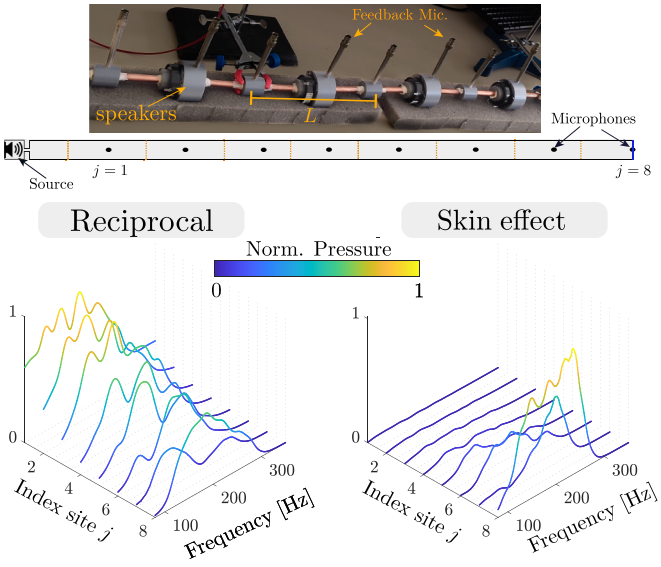

FIG. 3. The experimentally measured pressure as a function of the index site j and the frequency f, for a symmetrical ($t = 1$, bottom left) and asymmetrical ($t = 3.7$, bottom right) hopping, where the system is excited from the left side at $j = 0$. Mic., microphone, Norm., normalized.

derivation of the transfer matrix, please see Supplemental Material (SM) [54].

To confirm the nonreciprocity of the unit cell, the experimentally measured determinant of the transfer matrix $\det(\mathbf{M})$ is displayed as a function of the frequency in Fig. 2(b). In the absence of a feedback loop $G = 0$, the system is reciprocal [i.e., $t = \det(\mathbf{M}) = 1$] since the loudspeaker behaves as a passive resonator. However, if a gain $G \neq 0$ is applied, the reciprocity is broken, and the hopping term t becomes nonunitary, thereby favoring propagation in one direction. For the measurements shown in Fig. 2(b) we have tuned the gain such that $t = 3.7$, which would lead to a right-side localization with $(w_E > 1)$. Furthermore, one can see that the hopping factor is frequency independent and thus the mapping is broadband.

A finite-size lattice composed of $N = 8$ cells is constructed, and the two ends of the total waveguide are closed with rigid walls. Such a setup corresponds to Dirichlet boundary conditions for the acoustic flux and thus to an OBC HN model. We excite the system from the one end (left) and measure the pressure at equidistant points designated by $p(\omega, x_j)$ as shown at the top of Fig. 3. The bottom panels of Fig. 3 depict the normalized magnitude of the measured acoustic pressure at different sites as a function of frequency. Starting with the reciprocal case ($t = 1$), the acoustic pressure signal response is found to be strong only within the interval $f \in [120, 300]$ Hz, which is the first allowed band of the periodic lattice. Furthermore, the field appears to have greater amplitude near the source due to the strong damping (mainly caused by the loudspeakers), since away from the source the wave is rapidly dissipated.

On the other hand, by turning on the feedback gain and reaching a value of the asymmetric hopping $t = 3.7$, we clearly see the appearance of the non-Hermitian skin effect at the opposite boundary of the system. This means that despite the high damping, and excitation from the left-hand side, the excited bulk modes exhibit a strong localization on the right side. In fact, the amplification ratio from the first site, $j = 1$, to site $j = N$ is as high as $p(x_N)/p(x_1) = 120$. Note that the accumulation of energy on the right-hand side is persistent for all frequencies in this band confirming the fact that all modes exhibit the skin effect. Additionally, this amplification is in quantitative agreement with the OBC solutions where the amplification ratio for the modes is $\sim t^{N/2}$. *Experimental transition from PBCs to OBCs.* As mentioned before, many of the properties of topological non-Hermitian systems lie in the complex spectrum. As such, here we focus on measuring the complex eigenfrequencies f_n of our setup, which can be obtained by fitting the frequency response using a dedicated algorithm [55,56].

Figures 4(a)–4(c) show the measured eigenfrequencies in the complex plane for the acoustic waveguide with OBCs. The reciprocal ($t = 1$) and nonreciprocal ($t = 1.35$) systems have seven acoustic modes and, as predicted by the theory, form an arc lying in the negative imaginary part of the complex plane. For the HN model the OBC spectrum always lies on the real axis for any value of t. However, here we see that by increasing the gain (thus t) the modes are pushed towards the real axis. This property, which is embedded in the proposed mapping, reveals the fact that adding gain to the system allows one to better compensate losses. To further reveal the NHSE, we measure the pressure field at different positions of the waveguide for the corresponding eigenfrequencies.

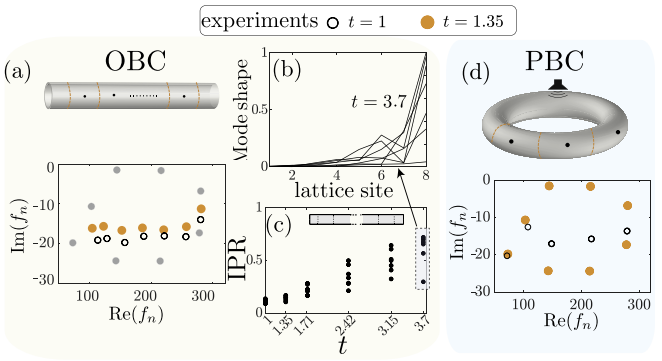

FIG. 4. (a) Complex eigenfrequencies of the problem in the OBC configuration, for $t = 1$ (open black circles) and $t = 1.35$ (solid orange circles), and for the PBCs at $t = 1.35$ (gray circles). (b) Mode shape of the OBC configuration for $t = 3.7$. (c) The inverse participation ratio of each mode shape as a function of the hopping factor t in the OBC configuration. (d) Complex eigenfrequencies in the PBC configuration, for $t = 1$ (open black circles) and $t = 1.35$ (solid orange circles).

An example of the mode shape for $t = 3.7$ is shown in Fig. 4(b) where the energy is clearly localized predominantly on the right boundary ($j = 8$). Moreover, we plot the experimentally obtained inverse participation ratio (IPR), $\sum_k |p(x_k)|^2/(\sum_k |p(x_k)|)^2$, as a function of t in Fig. 4(c). This ratio quantifies the localization level of the eigenmodes; for instance, values of IPR $= 1$ and IPR $= 0$ indicate a total localization at one site and full delocalization, respectively. As anticipated, the present results indicate that the increase in the hopping factor leads to a stronger localization of the eigenmodes on the right side of the system.

Importantly, our modeling predicts that the proposed acoustic device can have stable configurations not only with OBCs but also using PBCs. This is possible due to the inherent losses and their accurate modeling. We build such a device using a looped waveguide as shown in the top panel of Fig. 4(d). In the bottom panel of Fig. 4(d) we show the experimental eigenfrequencies for the PBC waveguide $N = 8$. In the reciprocal case with $t = 1$, five eigenfrequencies are identified; among them, three are degenerate with multiplicity 2 due to the angular symmetry. On the other hand, in the nonreciprocal case $t = 1.35$, the degenerate modes split in pairs, and the spectrum forms a closed loop in the complex plane indicated by the solid orange circles in the bottom panel of Fig. 4(d). An important aspect of the proposed acoustic system is that as expected, there is a maximum value of the gain, after which some modes become unstable.

Another interesting aspect of the proposed system is that it allows one to study experimentally the transition from PBCs to OBCs. This transition has been the subject of several studies since it gives insights into the sensitivity of the underlying spectrum under changes in the boundary conditions. Experimentally, it has only been observed in discrete lattices [31], but not in a continuous wave system. Here, we achieve the transition in a rather natural way by adding a thin diaphragm of radius r_d inside the looped waveguide of radius r_w and progressively reducing the ratio $r = r_d/r_w$. In the bottom panel of Fig. 5(a) we plot the experimentally obtained spectrum in the complex plane for various values of r between PBCs ($r = 1$) and OBCs ($r = 0$). The first row corresponds to a relatively small gain $t = 1.35$, and the transition is explicitly demonstrated for all the ranges of the diaphragm radius. As the radius decreases, the ellipse gradually shrinks until it transforms into an arc for the OBCs. This transition is clearly visible for various values of t as shown in Fig. 5(a). In addition,

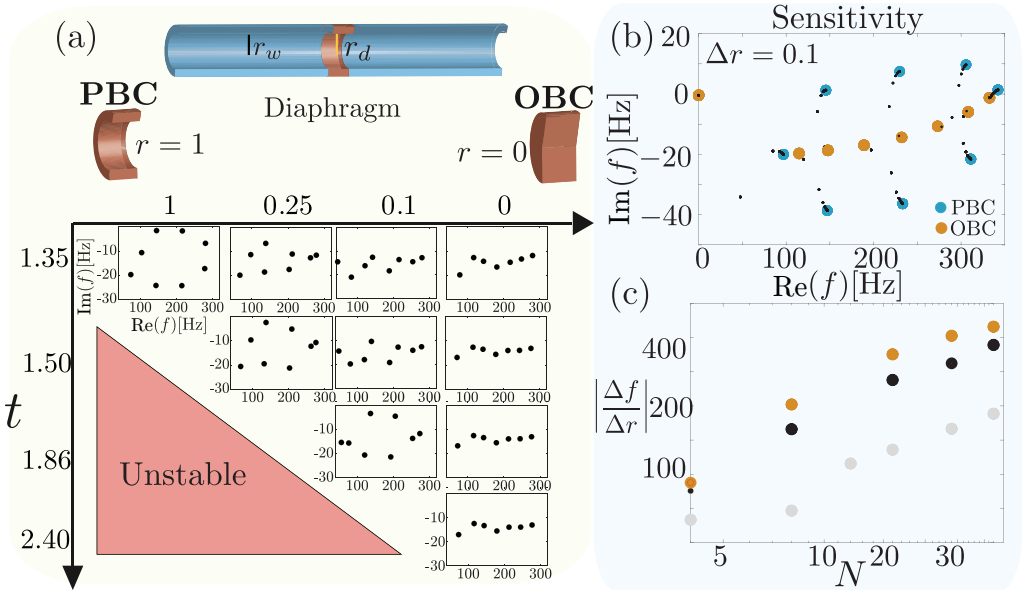

FIG. 5. (a) Top: a schematic of the diaphragm used in experiments inside the waveguide. Bottom: the eigenfrequencies obtained from experimental results for different values of the nonreciprocal hopping t and the ratio r. (b) The transition from PBCs to OBCs obtained using the experimentally fitted transfer matrix. (c) The exponential sensitivity of the absolute value of the eigenfrequency as a function of the system size.

as predicted by the theory, by increasing the hopping factor for a fixed radius ratio (e.g., the column for 0.1), the ellipse expands, which is a characteristic of the HN model.

The red shaded region in the bottom panel of Fig. 5(a) indicates the values of t where the system becomes unstable, i.e., at least one mode has an imaginary part crossing the real axis. In fact, in the marginal case of $t = 2.4$, by opening a small hole (10% of the waveguide radius) the otherwise stable OBC configuration abruptly becomes unstable. This motivates us to follow recent results showing the exponential sensitivity of the HN with respect to the system size l [20,24,57] and explore this aspect for our system. To do so, we investigate the sensitivity semianalytically using the experimentally obtained transfer matrix M_{expt}. In particular, we use an analytical 1D model (see SM) including the effect of a thin diaphragm [58,59] and fit it to the experimentally obtained elements of M_{expt}. To find the corresponding eigenfrequencies of the system with PBCs, one can calculate the solutions of $\det(M_d M_{\text{expt}}^N - I) = 0$ (see Supplemental Material [54]). Figure 5(b) exhibits the eigenfrequencies of a system with $N = 8$ and $t = 1.5$ [corresponding to the second row in the bottom panel of Fig. 5(a)]. Here we vary the ratio r by increments of 0.1. What we observe is that with $r = 0.1$ the eigenfrequencies have slightly shifted as observed in the experiments. Then for $r > 0.2$ a large ellipse has been formed in the complex plane indicating a strong change in the eigenfrequencies. To further quantify this sensitivity, we have calculated the change in the absolute value of the frequency for the mode in the center of the ellipse for a change in the ratio $\Delta r = 0.1$. The results for three different values of t are shown in Fig. 5(c) in a logarithmic scale. It is clear that the proposed acoustic system is indeed exponentially sensitive to its size.

Conclusion. In this Research Letter, an exact mapping of the Hatano-Nelson model to one-dimensional nonreciprocal continuous systems is presented. The mapping is achieved solely by using a transfer matrix approach and can be applied to a plenitude of systems, provided that nonreciprocity can be implemented for the given device. The experimental results show the emergence of the non-Hermitian skin effect once an asymmetric hopping is achieved, and by analyzing the complex frequency of the acoustic mode, the theoretical model is validated. Finally, while using diaphragms of different hole sizes, the transition from PBCs to OBCs and the subsequent exponential sensitivity to the system size are exhibited. Using the proposed method, many other variants of the NH model can be constructed in continuous media, including various nonreciprocal topological models or higher-dimensional models which profit from the interplay between topology and non-Hermiticity.

Acknowledgments. V.A. acknowledges financial support from the NoHeNA project funded under the program Etoiles Montantes of the Region Pays de la Loire. V.A. is supported by EU H2020 ERC StG "NASA" Grant Agreement No. 101077954.

[1] Y. Ashida, Z. Gong, and M. Ueda, Non-Hermitian physics, Adv. Phys. **69**, 249 (2020).

[2] R. El-Ganainy, K. G. Makris, M. Khajavikhan, Z. H. Musslimani, S. Rotter, and D. N. Christodoulides, Non-Hermitian physics and $\mathcal{PT}$ symmetry, Nat. Phys. **14**, 11 (2018).

[3] C. M. Bender and S. Boettcher, Real spectra in non-Hermitian Hamiltonians having $\mathcal{PT}$ symmetry, Phys. Rev. Lett. **80**, 5243 (1998).

[4] C. M. Bender, M. Berry, and A. Mandilara, Generalized $\mathcal{PT}$ symmetry and real spectra, J. Phys. A: Math. Gen. **35**, L467 (2002).

[5] Z.-P. Liu, J. Zhang, Ş. K. Özdemir, B. Peng, H. Jing, X.-Y. Lü, C.-W. Li, L. Yang, F. Nori, and Y.-X. Liu, Metrology with $\mathcal{PT}$-symmetric cavities: Enhanced sensitivity near the $\mathcal{PT}$-phase transition, Phys. Rev. Lett. **117**, 110802 (2016).

[6] M.-A. Miri and A. Alù, Exceptional points in optics and photonics, Science **363**, eaar7709 (2019).

[7] J. Wiersig, Review of exceptional point-based sensors, Photonics Res. **8**, 1457 (2020).

[8] W. Chen, Ş. K. Özdemir, G. Zhao, J. Wiersig, and L. Yang, Exceptional points enhance sensing in an optical microcavity, Nature (London) **548**, 192 (2017).

[9] Y. Aurégan and V. Pagneux, $\mathcal{PT}$-symmetric scattering in flow duct acoustics, Phys. Rev. Lett. **118**, 174301 (2017).

[10] S. Longhi, $\mathcal{PT}$-symmetric laser absorber, Phys. Rev. A **82**, 031801(R) (2010).

[11] Y. Chong, L. Ge, and A. D. Stone, $\mathcal{PT}$-symmetry breaking and laser-absorber modes in optical scattering systems, Phys. Rev. Lett. **106**, 093902 (2011); **108**, 269902(E) (2012).

[12] G. Poignand, C. Olivier, and G. Penelet, Parity-time symmetric system based on the thermoacoustic effect, J. Acoust. Soc. Am. **149**, 1913 (2021).

[13] Z. J. Wong, Y.-L. Xu, J. Kim, K. O'Brien, Y. Wang, L. Feng, and X. Zhang, Lasing and anti-lasing in a single cavity, Nat. Photonics **10**, 796 (2016).

[14] Z. Lin, H. Ramezani, T. Eichelkraut, T. Kottos, H. Cao, and D. N. Christodoulides, Unidirectional invisibility induced by $\mathcal{PT}$-symmetric periodic structures, Phys. Rev. Lett. **106**, 213901 (2011).

[15] A. Mostafazadeh, Invisibility and $\mathcal{PT}$ symmetry, Phys. Rev. A **87**, 012103 (2013).

[16] C. C. Wanjura, M. Brunelli, and A. Nunnenkamp, Correspondence between non-Hermitian topology and directional amplification in the presence of disorder, Phys. Rev. Lett. **127**, 213601 (2021).

[17] S. Longhi, Self-healing of non-Hermitian topological skin modes, Phys. Rev. Lett. **128**, 157601 (2022).

[18] S. Weidemann, M. Kremer, T. Helbig, T. Hofmann, A. Stegmaier, M. Greiter, R. Thomale, and A. Szameit, Topological funneling of light, Science **368**, 311 (2020).

[19] E. Edvardsson and E. Ardonne, Sensitivity of non-Hermitian systems, Phys. Rev. B **106**, 115107 (2022).

[20] J. C. Budich and E. J. Bergholtz, Non-Hermitian topological sensors, Phys. Rev. Lett. **125**, 180403 (2020).

[21] A. McDonald and A. A. Clerk, Exponentially-enhanced quantum sensing with non-Hermitian lattice dynamics, Nat. Commun. **11**, 5382 (2020).

[22] F. Koch and J. C. Budich, Quantum non-Hermitian topological sensors, Phys. Rev. Res. **4**, 013113 (2022).

[23] M. Parto, C. Leefmans, J. Williams, and A. Marandi, Enhanced sensitivity via non-Hermitian topology, arXiv:2305.03282.

[24] H. Yuan, W. Zhang, Z. Zhou, W. Wang, N. Pan, Y. Feng, H. Sun, and X. Zhang, Non-Hermitian topolectrical circuit sensor with high sensitivity, Adv. Sci. **10**, 2301128 (2023).

[25] E. J. Bergholtz, J. C. Budich, and F. K. Kunst, Exceptional topology of non-Hermitian systems, Rev. Mod. Phys. **93**, 015005 (2021).

[26] N. Okuma and M. Sato, Non-Hermitian topological phenomena: A review, Annu. Rev. Condens. Matter Phys. **14**, 83 (2023).

[27] N. Okuma, K. Kawabata, K. Shiozaki, and M. Sato, Topological origin of non-Hermitian skin effects, Phys. Rev. Lett. **124**, 086801 (2020).

[28] X. Zhang, T. Zhang, M.-H. Lu, and Y.-F. Chen, A review on non-Hermitian skin effect, Adv. Phys.: X **7**, 2109431 (2022).

[29] R. Lin, T. Tai, L. Li, and C. H. Lee, Topological non-Hermitian skin effect, Front. Phys. **18**, 53605 (2023).

[30] K. Xu, X. Zhang, K. Luo, R. Yu, D. Li, and H. Zhang, Coexistence of topological edge states and skin effects in the non-Hermitian Su-Schrieffer-Heeger model with long-range nonreciprocal hopping in topoelectric realizations, Phys. Rev. B **103**, 125411 (2021).

[31] T. Helbig, T. Hofmann, S. Imhof, M. Abdelghany, T. Kiessling, L. Molenkamp, C. Lee, A. Szameit, M. Greiter, and R. Thomale, Generalized bulk–boundary correspondence in non-Hermitian topolectrical circuits, Nat. Phys. **16**, 747 (2020).

[32] S. Liu, R. Shao, S. Ma, L. Zhang, O. You, H. Wu, Y. J. Xiang, T. J. Cui, and S. Zhang, Non-Hermitian skin effect in a non-Hermitian electrical circuit, Research **2021**, 5608038 (2021).

[33] L. Zhang, Y. Yang, Y. Ge, Y.-J. Guan, Q. Chen, Q. Yan, F. Chen, R. Xi, Y. Li, D. Jia, S.-Q. Yuan, H.-X. Sun, H. Chen, and B. Zhang, Acoustic non-Hermitian skin effect from twisted winding topology, Nat. Commun. **12**, 6297 (2021).

[34] Z. Gu, H. Gao, H. Xue, J. Li, Z. Su, and J. Zhu, Transient non-Hermitian skin effect, Nat. Commun. **13**, 7668 (2022).

[35] N. Hatano and D. R. Nelson, Localization transitions in non-Hermitian quantum mechanics, Phys. Rev. Lett. **77**, 570 (1996).

[36] S. Yao and Z. Wang, Edge states and topological invariants of non-Hermitian systems, Phys. Rev. Lett. **121**, 086803 (2018).

[37] Q. Zhou, J. Wu, Z. Pu, J. Lu, X. Huang, W. Deng, M. Ke, and Z. Liu, Observation of geometry-dependent skin effect in non-Hermitian phononic crystals with exceptional points, Nat. Commun. **14**, 4569 (2023).

[38] G. Penelet, V. Pagneux, G. Poignand, C. Olivier, and Y. Aurégan, Broadband nonreciprocal acoustic scattering using a loudspeaker with asymmetric feedback, Phys. Rev. Appl. **16**, 064012 (2021).

[39] F. K. Kunst and V. Dwivedi, Non-Hermitian systems and topology: A transfer-matrix perspective, Phys. Rev. B **99**, 245116 (2019).

[40] K. Zhang, Z. Yang, and C. Fang, Correspondence between winding numbers and skin modes in non-Hermitian systems, Phys. Rev. Lett. **125**, 126402 (2020).

[41] B. Peng, Ş. K. Özdemir, M. Liertzer, W. Chen, J. Kramer, H. Yılmaz, J. Wiersig, S. Rotter, and L. Yang, Chiral modes and directional lasing at exceptional points, Proc. Natl. Acad. Sci. USA **113**, 6845 (2016).

[42] H.-Z. Chen, T. Liu, H.-Y. Luan, R.-J. Liu, X.-Y. Wang, X.-F. Zhu, Y.-B. Li, Z.-M. Gu, S.-J. Liang, H. Gao, L. Lu, L. Ge, S. Zhang, J. Zhu, and R.-M. Ma, Revealing the missing dimension at an exceptional point, Nat. Phys. **16**, 571 (2020).

[43] A. Hashemi, S. Rezaei, S. Özdemir, and R. El-Ganainy, New perspective on chiral exceptional points with application to discrete photonics, APL Photonics **6**, 040803 (2021).

[44] C. Olivier, A. Maddi, G. Poignand, and G. Penelet, Asymmetric transmission and coherent perfect absorption in a periodic array of thermoacoustic cells, J. Appl. Phys. **131**, 244701 (2022).

[45] H. Nassar, B. Yousefzadeh, R. Fleury, M. Ruzzene, A. Alù, C. Daraio, A. N. Norris, G. Huang, and M. R. Haberman, Nonreciprocity in acoustic and elastic materials, Nat. Rev. Mater. **5**, 667 (2020).

[46] R. Fleury, D. L. Sounas, C. F. Sieck, M. R. Haberman, and A. Alù, Sound isolation and giant linear nonreciprocity in a compact acoustic circulator, Science **343**, 516 (2014).

[47] B.-I. Popa and S. A. Cummer, Non-reciprocal and highly nonlinear active acoustic metamaterials, Nat. Commun. **5**, 3398 (2014).

[48] Y. Zhai, H.-S. Kwon, and B.-I. Popa, Active Willis metamaterials for ultracompact nonreciprocal linear acoustic devices, Phys. Rev. B **99**, 220301(R) (2019).

[49] N. Geib, A. Sasmal, Z. Wang, Y. Zhai, B.-I. Popa, and K. Grosh, Tunable nonlocal purely active nonreciprocal acoustic media, Phys. Rev. B **103**, 165427 (2021).

[50] Z. Chen, Y. Peng, H. Li, J. Liu, Y. Ding, B. Liang, X.-F. Zhu, Y. Lu, J. Cheng, and A. Alù, Efficient nonreciprocal mode transitions in spatiotemporally modulated acoustic metamaterials, Sci. Adv. **7**, eabj1198 (2021).

[51] C. Shen, X. Zhu, J. Li, and S. A. Cummer, Nonreciprocal acoustic transmission in space-time modulated coupled resonators, Phys. Rev. B **100**, 054302 (2019).

[52] C. Rasmussen, L. Quan, and A. Alù, Acoustic nonreciprocity, J. Appl. Phys. **129**, 210903 (2021).

[53] A. Maddi, C. Olivier, G. Poignand, G. Penelet, V. Pagneux, and Y. Aurégan, Frozen sound: An ultra-low frequency and ultra-broadband non-reciprocal acoustic absorber, Nat. Commun. **14**, 4028 (2023).

[54] See Supplemental Material at http://link.aps.org/supplemental/10.1103/PhysRevResearch.6.L012061 for a detailed derivation of the transfer matrix, the solutions of $\det(M_d M_{\text{expt}}^N - I) = 0$, and details of the analytical 1D model.

[55] M. S. Allen and J. H. Ginsberg, A global, single-input–multi-output (SIMO) implementation of the algorithm of mode isolation and application to analytical and experimental data, Mech. Syst. Signal Process. **20**, 1090 (2006).

[56] B. Peeters, H. Van der Auweraer, P. Guillaume, and J. Leuridan, The PolyMAX frequency-domain method: a new standard for modal parameter estimation? Shock Vib. **11**, 395 (2004).

[57] Y. Liu, Y. Zeng, L. Li, and S. Chen, Exact solution of the single impurity problem in nonreciprocal lattices: Impurity-induced size-dependent non-Hermitian skin effect, Phys. Rev. B **104**, 085401 (2021).

[58] J. Kergomard and A. Garcia, Simple discontinuities in acoustic waveguides at low frequencies: Critical analysis and formulae, J. Sound Vib. **114**, 465 (1987).

[59] T. Herdtle, J. S. Bolton, N. N. Kim, J. H. Alexander, and R. W. Gerdes, Transfer impedance of microperforated materials with tapered holes, J. Acoust. Soc. Am. **134**, 4752 (2013).